KSCE Journal of Civil Engineering (2019) 23(1):46-55
Copyright ⓒ2019 Korean Society of Civil Engineers
DOI 10.1007/s12205-018-0942-5

Geotechnical Engineering

pISSN 1226-7988, eISSN 1976-3808
www.springer.com/12205

Axial Resistance of Bored Piles Socketed into Soft Rock

Xiao-yu Chen*, Ming-yi Zhang, and Xiao-yu Bai*****

Received July 15, 2017/Revised 1st: October 14, 2017, 2nd: January 30, 2018, 3rd: April 19, 2018/Accepted July 26, 2018/Published Online November 30, 2018

Abstract

Three fully-instrumented full-scale static load tests were conducted on three 0.8-m-diameter bored piles socketed at 3.2 m deep into argillaceous siltstone (1.6 and 1.6 deep into strong and medium decomposed siltstones, respectively) in Qingdao, China. About 50% of head load was transmitted and supported by base resistance at the end of the tests. Totally 53 test piles socketed into soft rock with unconfined compressive strength less than 20 MPa in Qingdao were reviewed. The measured side resistance along shaft socked into rock was compared with prediction using empirical methods in literatures based on database from Qingdao projects.

Keywords: *rock-socket pile, side resistance, axial force*

1. Introduction

Rock-socketed and in-site-cast bored piles are widely used owing to their high bearing capacity, small displacement and easy construction. This type of piles has been preferred in Qingdao recently due to the quick development of reclaimed lands with high-density building works off the coast (Shi and Lin, 1994). However, the uncertainty and complexity of the base rock bring about new challenges for designers to achieve more beneficial results (Kulkarni and Dewaikar, 2016). Hence, the force transfer mechanism and properties should be further understood.

Model and theoretical analyses have been carried out to investigate various aspects of rock-socketed bored piles, such as the effects of rock/pile surface roughness on piles (Gong *et al.*, 2011; Xing *et al.*, 2014), pile size effect by finite element (Ye *et al.*, 2004; Zhao *et al;*, 2009), estimation of head displacement, and bearing capacity (Dai *et al.*, 2013; Zhang, 2010). Fatahi *et al.* (2014) investigated the effects of the initial stress state and interface parameters on the performance of laterally loaded pile system by modified finite element model. The results indicated that the coefficient of lateral earth pressure K_o exerts important influence on displacement, depth-bending moment, but has limited effect on initial modulus, and the secant modulus of subgrade reaction increases as K_o increases. However, these analyses ignored several important aspects: (1) The blurry module scale effect limits the accuracy of results; and (2) the gradual change between different weathering zones; and (3) erratic condition below rock. Accordingly, high-quality full-scale load tests are imperatively needed to clarify these problems in rock-socketed piles.

Some field tests on well-instrumented bore and rock-socket piles as onshore foundation were carried out recently (Luo *et al*, 2014., Gong *et al*, 2011., Wang *et al*, 2015). These tests reveal three key observations different from full-soil-socketed piles: (1) Less than 30% of head loading was provided by end resistance during load tests; (2) up to 25% of shaft head load can be supported by the shaft base, even at relatively small shaft head displacement; (3) rock-socket piles performed well in bearing capacity, despite socking into soft rock. Since site coefficients are not provided in literatures (Hoek *et al.*, 2002; Charles *et al.,* 2001; Charif *et al.*, 2010), the application of these findings into Qingdao cannot be guaranteed.

In this study, the instrument, installation, and static loading tests of three 0.8-m-diameter rock-socketed bored piles driven into 15 m deep in multilayered soil and 3 m deep in argillaceous siltstone were reported. This study is aimed to (1) discuss the response of rock-socket piles under vertical compression and (2) assess the existing estimations of side resistance along shaft socketed into rock based on Qingdao projects. Two innovations are presented in the paper (1) the high-quality, well-recorded and large-scale field tests were carried out on three piles to investigate the performance of rock-socketed pile under vertical compression and (2) a new model is creatively presented to predict the side friction along socket length based on the 53 testing piles in Qingdao.

2. Background

Qingdao, a coastal hilly city of Shandong province, China,

*M.Sc. Student, Civil Engineering Dept., Qingdao University of Technology, Qingdao 266000, China (E-mail: 15963256565@163.com)
**Professor, Civil Engineering Dept., Qingdao University of Technology, Qingdao 266000, China (E-mail: zmy58@163.com)
***Associate Professor, Civil Engineering Dept., Qingdao University of Technology, Qingdao 266000, China (Corresponding Author, E-mail: baixiaoyu538@163.com)

enjoys great ground conditions due to its low rock surface (depth of 0.5 to 10 m) and good mechanism parameters of upper soil (from quaternary system) except for backfill for reclamation. Sandstone and mudstone are widely distributed at the urban outskirts in Qingdao, while granite is ubiquitous in the urban center. In addition, the quick urbanization which requires buildings with high bearing capacity and low displacement increases the application of rock-socket piles. Hence, 99% of piles in Qingdao are rock-socketed (strong medium rock) and perform well in bearing capacity in recent years with diameter of 0.6–2 m and length of 5–30 m.

3. Test Program

3.1 Site Description

Field tests were carried out at a construction site in Qingdao, which was reclaimed from the sea. The site is relatively flat without obvious fluctuations. The location of the in-situ tests is shown in Fig. 1. A series of field tests and laboratory tests were conducted to measure and analyze the mechanism parameters about the soil and rock layer (Table 1).

The site is underlined consecutively with a gravel fill layer, a clay fill layer, strong weathered rock and medium weathered rock. The gravel fill layer is mainly composed of gravels at a depth of 9–12 m, with N ranging from 6.8–9. The clay-fill layer consists of < 20% clay with shell fragment at depth of 3–5 m, with N varying from 1–3. Below the clay-fill layer lies the strong weathered rock with small thickness and destructibility at depth of 2 to 3 m. The medium weathered rock is almost intact with limited fractures at the depth of 3 m. Unconfined compressive strength of an intact was detected from point-load tests. The base of the test pile was found at the medium weathered rock at depth of 1.6 m (equal to 2*D*).

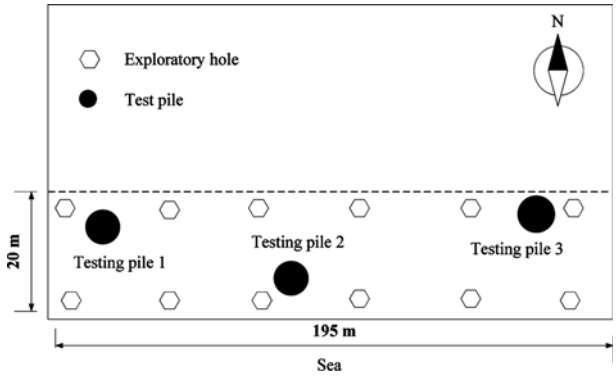

Fig. 1. Location of Field Test

Table 1. Soils and Rocks Parameters

Layers	f_{ak} /kPa	E /MPa	γ /(kN/m)	φ /(°)	UCS /MPa
Fill (gravel)			20	30	
Fill (clay)	40-60		18	18	
SD argillaceous siltstone	500	30	23	23	3.5
MD argillaceous siltstone	2000	5000	24	24	11.5

Note: f_{ak} is the ground bearing capacity (kPa); E is the deformation modulus (MPa); γ is the natural unit weight (kN/m), φ is the internal friction angle; UCS is the average unconfined compressive strength of intact rock (MPa). SD means strong decomposed; MD means medium decomposed.

3.2 Pile Installation and Instrument

Three well-instrumented rock-socket bored piles were employed on field tests. The average valid length and diameter of the test piles were 18 and 0.8 m, respectively (with rocked depth of 1.6 and 1.6 m for strong and medium decomposed rocks respectively). The ultimate bearing capacity of the three test piles was estimated at 8000 kN in accordance with Chinese Technical Code for Building Pile Foundations (JGJ94-2014). End post-pouring was conducted 2 days after installation. The basic information of the

Table 2. Parameters of Testing Piles

No.	Valid length/m	Socked length/m	Diameter/ m	Filling coefficient	Filling date	Post-Pouring date
BP1	17.5	3.2	0.8	1.51	9.25	9.27
BP2	18	3.2	0.8	1.59	9.25	9.27
BP3	18.5	3.2	0.8	1.57	9.25	9.27

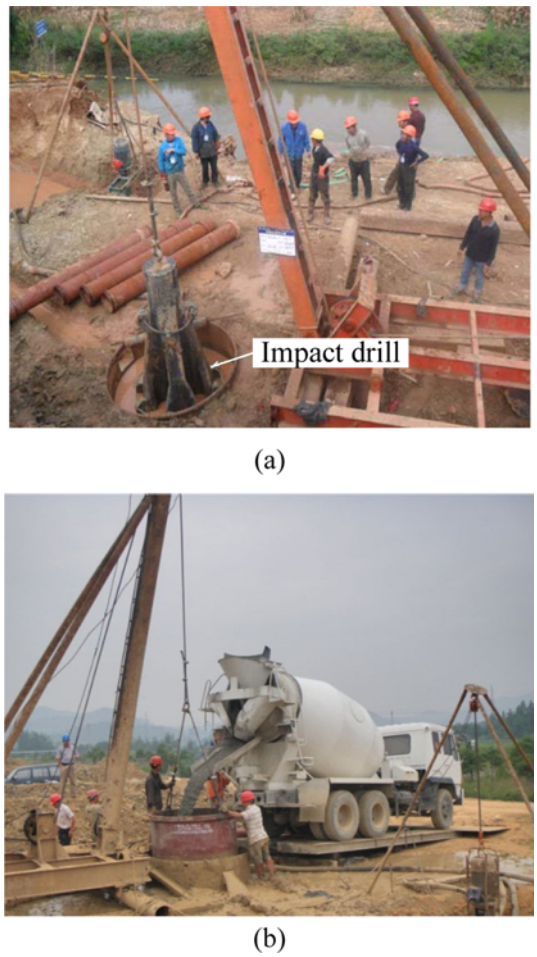

(a)

(b)

Fig. 2. Photos of Pile Installation

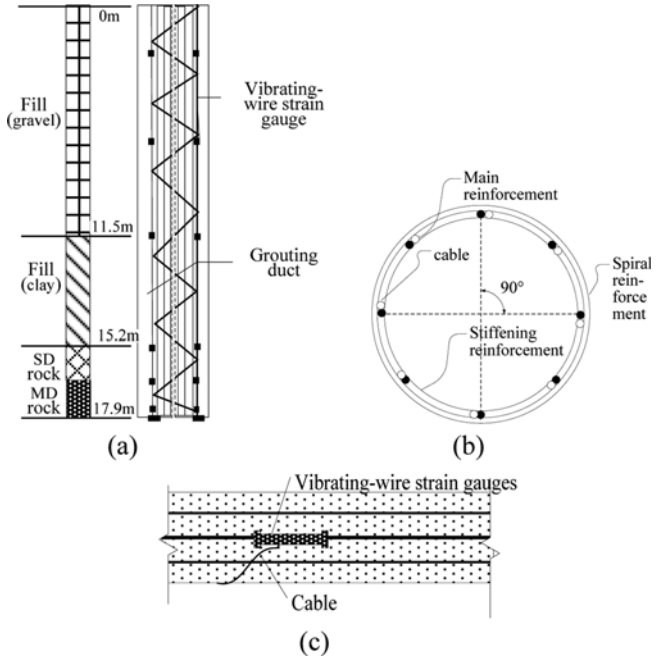

Fig. 3. Layout and Installation of Strain Gauges: (a) Layout of Strain Gauges along Shaft; (b) Cross Section of Piles with Sensors, (c) Installation of Strain Gauges

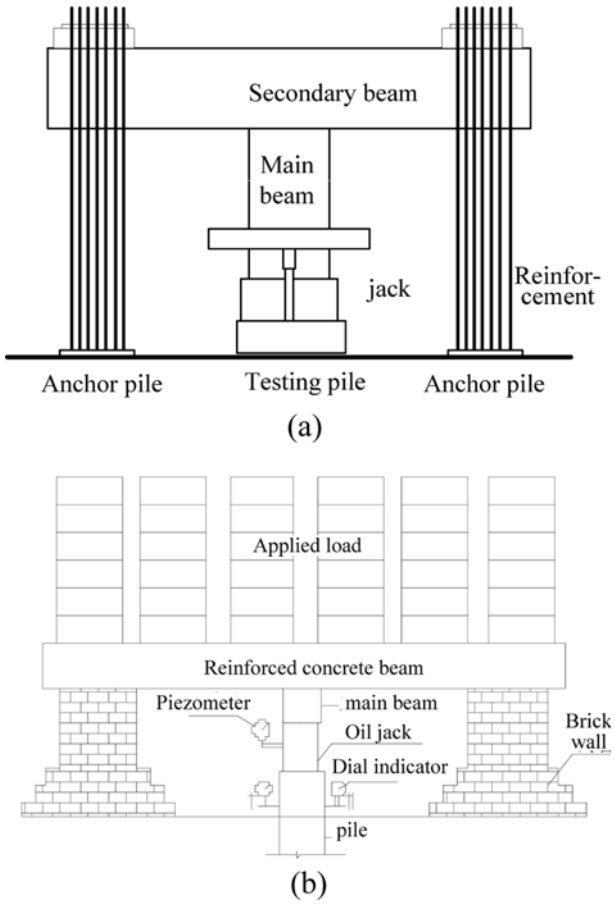

Fig. 4. View of Reaction System: (a) Anchor-pile System, (b) Concrete-block System

test piles is showed in Table 2. The filling coefficient is defined as the ratio of actual to theoretical concrete volume.

The test piles were bored and installed using an impact drilling technique (Fig. 2). First, the pile casing was placed at the designated location to avoid collapse during installation. Then the impact drill with a certain quality was lifted by the crane and suddenly put underground so the impact energy could squeeze the soil or broken rock to form a hole. After that, the hole was cleared by slurry and then installed with a reinforcement cage by the crane. Finally, the pile casing was put out and concrete was filled in.

The test piles were instrumented with vibrating wire strain gauges along the reinforcement cage to monitor the axial force distribution and transfer mechanism. Six groups of gauges were installed at different shaft surfaces (Fig. 3). Each level had four vibrating wire strains at an interval of 90° (Fig. 3(b)). All the stain gauges were located by coaxial butt welding (Fig. 3(c)). Near the pile base, the gauges were arranged around 0.5 m above the base to avoid damage. At the base of the shaft, reinforcement cage was installed two vibrating wire earth pressure sensors to monitor the base resistance during tests.

3.3 Static Loading Test

Two main reaction systems were used in Qingdao (Fig. 4). First, the anchor-pile reaction system with low cost and high safety (Fig. 4(a)) is widely used to provide high reaction force, while the available anchor piles around the test pile are equally needed. However, the anchor-pile would be pulled out sometimes owing to the weak bearing capacity compared to Jack's force. Second, the concrete block reaction (Fig. 4(b)) performs better in reacting loading, which is mainly applied under low bearing capacity due to the better ground condition required to support the heavy concrete block, which also needs high cost and adds construction difficulty. In this project where the high bearing capacity was needed and weak ground condition was performed, the second system was used given three reasons: (1) concrete block performed better without loss of efficacy; (2) anchor piles were not found at the site; (3) ground condition was improved by dynamic compaction before tests.

Static loading tests on three piles were performed in a local construction company on October 15 (30 days after concrete pouring and 28 days after end-post grouting). The static loading was applied vertically on the pile head by increasing the pressure in 4 hydraulic jacks, which were positioned between the pile head and reaction beam and generated from the concrete blocks above the beam. The applied head load was measured and recorded by a calibrated load cell, and the head displacement was monitored by four dial indicators symmetrically positioned above the pile head. The static loading tests were performed in accordance with Chinese Technical Code for Testing of Building Foundation Piles (JGJ106-2014) slowly maintained and without loading-unloading loops (Fig. 5). The maximum loading was

Fig. 5. Concrete Blocks and Reaction System of Static Load Test

more than 2 times the design load, and the loadings were 3200, 4800, 6400, 8000, 9600, 11200, 12800, 14400, 16000 and 17600 kN. According to the Chinese Technical Code for Testing of Building Foundation Piles (JGJ106-2014), when the head displacement is less than 0.1 mm within 60 min in two times, the next load could be applied.

4. Results and Discussion

4.1 Displacement Response

In general, the head displacement directly shows the bearing performance and transfer mechanism of piles compared with axial force, so mostly the ultimate status is defined based on the head displacements of both construction projects and research (Fellenius *et al.*, 2004; Kou *et al.*, 2016).

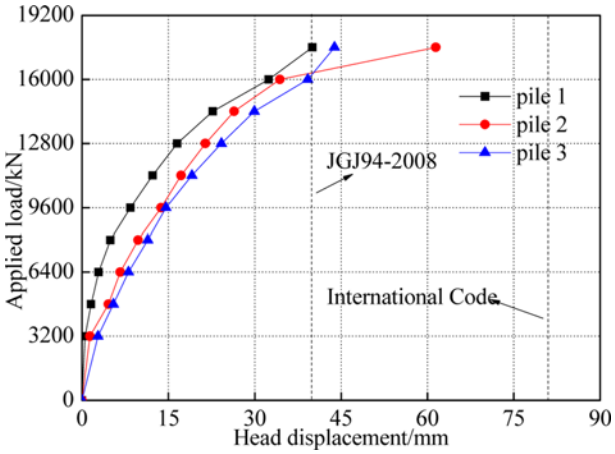

Fig. 6. Head Displacement-Applied Load Relationship

Table 3. Results of Compressive Static Load Tests

No.	Ultimate load/kN	Head displacement/ mm	Resilience /mm	Residual displacement/ mm	Resilience ratio/%
BP1	17600	42.42	19.32	23.1	0.46
BP2	17600	61.45			
BP3	17600	43.86	22.86	21	0.52

The displacement-load relationship for the test piles is shown in Fig. 6, with symbols of intermediate readings taken during the waiting time for stabilization of settlement caused by each load increase in accordance with JGJ106-2014.

The displacement-load response of three test piles was the slow type, without obvious fluctuations (Fig. 6 and Table 3). Head settlement increased nonlinearly from 0 to 61 mm with the rising growth rate along with the increasing applied load. As the test pile BP2 cannot stabilize at the head load of 17600 kN, resilience at each load cannot be obtained. Two test piles had better resilience performance, with resilience rate from 46% to 52% due to the better compression of pile shaft socketed into rock.

In most load tests, especially on rock-socketed piles, an ultimate load was inaccessible due to high construction cost and technological limitations. The ultimate load can be defined by different ultimate limit load criteria based on head displacement (Han *et al.*, 2016). Internationally, the ultimate load is defined when the head displacement arrives at 10% of pile diameter. The limit value can also be determined as the head settlement reaches or exceeds 40 mm in accordance with JGJ94-2008. Considering both project importance and use safety, we used the later definition here and defined the ultimate bearing capacity of three test piles as 16000 kN. However, it should be noticed this definition means the use of limit bearing capacity instead of the failure bearing capacity.

4.2 Axial Force Distribution

Six pairs of vibrating-wire strain gauges recorded axial force changes along steel cages at each load level. The average axial force along shaft F can be calculated as follows by assuming same deformation between steel bar and pile concrete:

$$P_s = K(f_0^2 - f_i^2) \tag{1}$$

$$P_c = P_s \times S_c \times E_c / (S_s \times E_s) \tag{2}$$

Because there are 12 main longitudinal steel bars embedded in each pile, the axial force along pile is as follows:

$$F = P_c + 12 \times P_s \tag{3}$$

where K is the constant of vibrating-wire strain gauges; f_0 is the initial frequency; f_i is the output frequency; P_s is the stress of single steel bar; P_c is the axial force of concrete; S_c is the cross-sectional area of pile; S_s is the cross-sectional area of single bar; E_c is the elastic modulus of concrete; E_s is the elastic modulus of steel bar; and F is the axial force of pile.

Figure 7 shows the profiles of axial force measured from strain gauges at different locations at each level. The three test piles performed in the same way during static compressive loading, which demonstrates the reliability of data and the flexibility of static compressive tests.

Axial force along test piles significantly decreased at depth of 15–18 m (strong and medium weathered rock layers), while the upon soil supported relatively small head load and the axial force

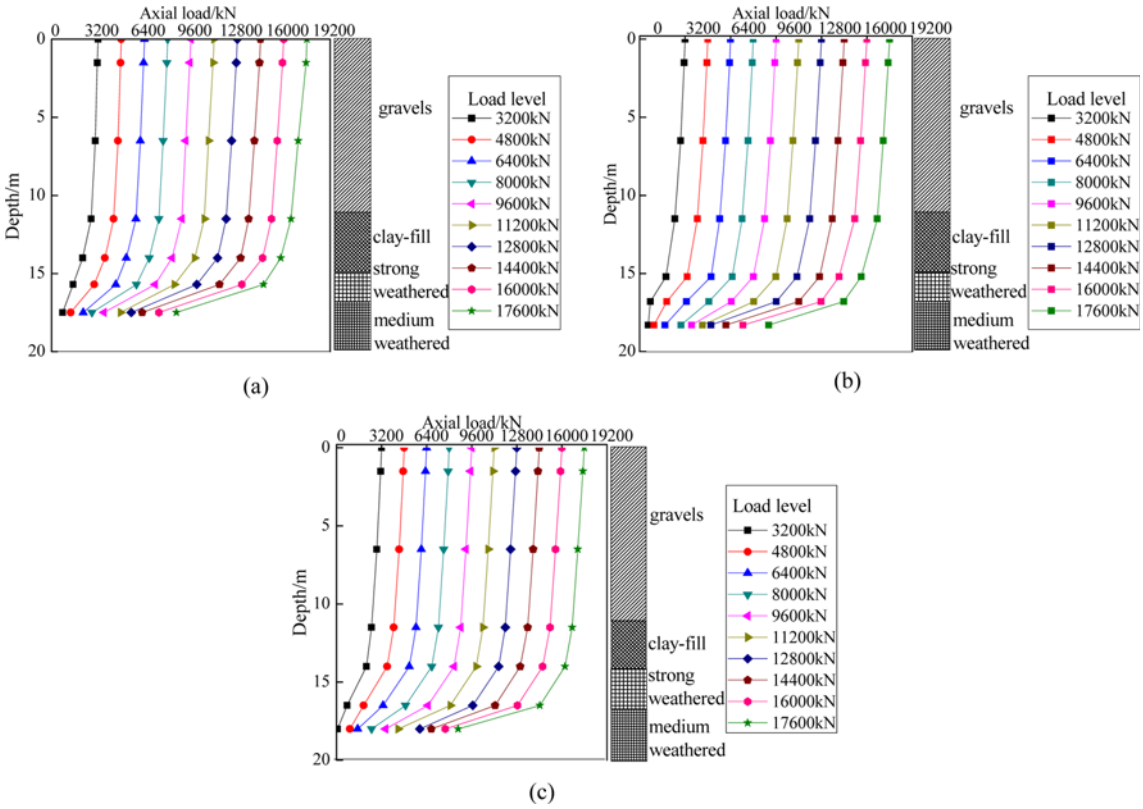

Fig. 7. Load Distribution in Test Piles: (a) BP1, (b) BP2, (c) BP3

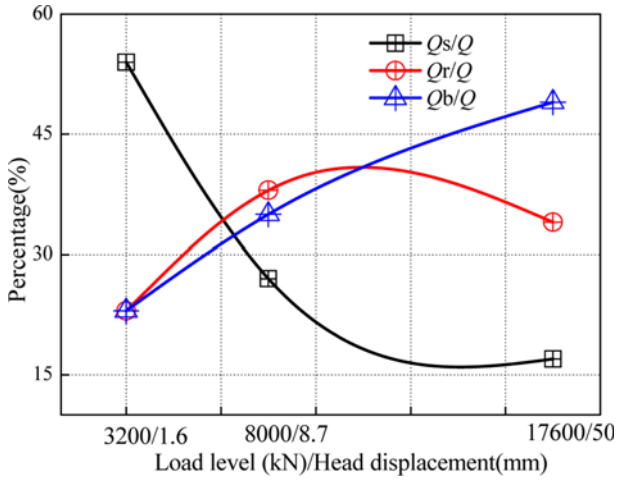

Where: Q: head load, Q_s: soil side resistance, Q_r: rock socket side resistance, Q_b: base resistance, S_i: pile head displacement

Fig. 8. Average Percentage of Axial Force supported by Shaft

curve along the soil almost kept parallel at each load level. The highest decreasing rate of axial force indicates the importance of reasonable estimation of rock side resistance along shaft. During the whole compressive loading, the ratio of base resistance to head load increased from 20% to 49%, while the ratio of soil resistance decreased to 19% (Fig. 8), which indicates a non-uniform mobilization of axial force along the depth.

The ratio of base resistance was 20% at initial stage (3200 kN) with low displacement of 1.6 mm, indicating a greater mobilization of base resistance even at a little displacement, which agrees with precious studies (Luo, 2014; Wang, 2015). When the pile test load reached the working load (8000 kN), the head displacement was no more than 9 mm, which suggests a high bearing capacity of the pile foundation. At the ultimate load, the percentage of head load supported and transmitted by base resistance was up to 49%, which was higher than previous reports for two reasons: (1) base resistance was not fully mobilized as limit load was not reached in previous studies; (2) soil upon piles provided less resistance in this study due to reclamation.

4.3 Side Resistance Distribution in Test Piles

Side resistance could be calculated from axial force measured from strain gauges and construction pile size gotten from drill holes around test piles. The formula assumes the load is distributed uniformly along the pile shaft between strain gauges (Yan, 2015):

$$q_i = (N_i - N_{i-1}) / (h_i U_p) \tag{4}$$

where q_i is the average side resistance of layer i; N_i and N_{i-1} are axial forces upon or below layer i, respectively; h_i is the thickness of layer i; and U_p is the perimeter of test piles at layer i.

The local side resistance at each load level of test piles was plotted against the normalized head displacement w/D (head displacement / pile diameter) in Fig. 9. Data show side friction increased as the normalized displacement was intensified through

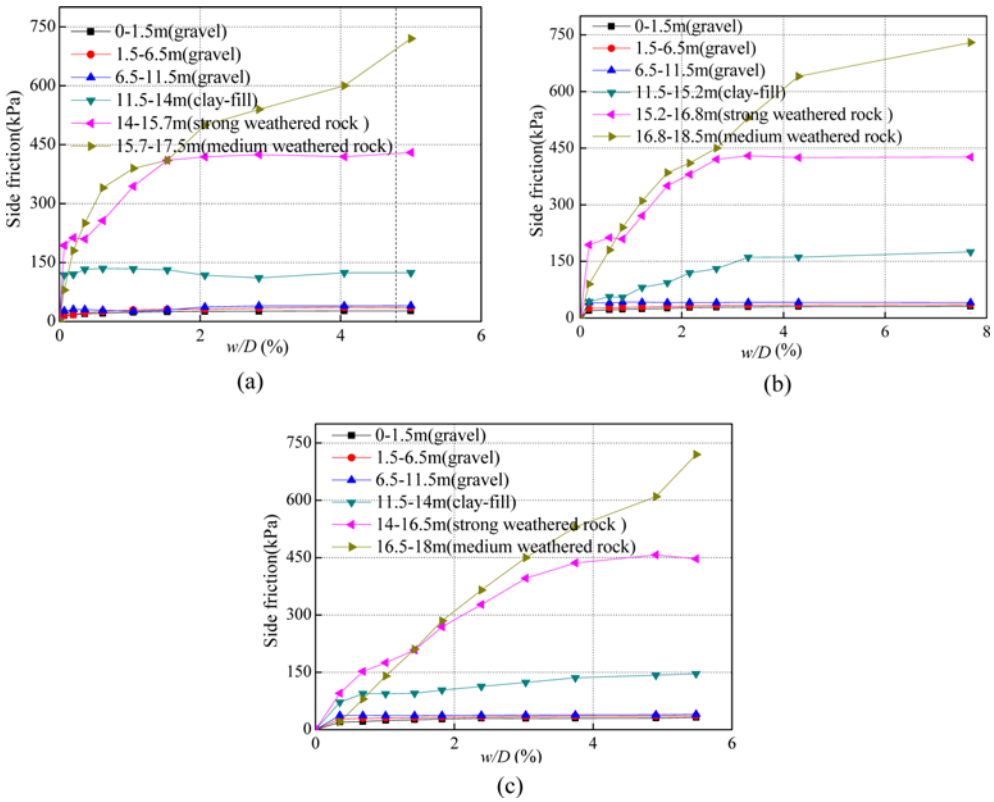

Fig. 9. Side Resistance Distribution of Testing Piles: (a) BP1, (b) BP2, (c) BP3

the compressive static tests. However, it's possible for the weak rock get degraded and its cohesive force get decreased when higher load is applied to the pile according to the research conducted by Lam Nguyen (Nguyen *et al.*, 2017), which the cementation effects in cement soil decreases due to the degradation of cementation bonds as the mean effective stress increases beyond the initial yield stress. The increasing side friction of medium weathered rock at the end of the tests indicated the mobilization of test piles was insufficient while other layers reached the ultimate shaft resistances.

The deeper piles indicate a larger shaft resistance during the tests, the average side resistance at the end of the tests was up to 730 kPa at medium weathered rock, 420–450 kPa at strong weathered rock, 160–180 kPa at the clay-fill layer and 40 kPa at gravel. The ultimate shear resistance along shaft socketed into rock was around 15 times of gravels and 4 times of the clay layer.

4.4 Estimation and Assessment of Side Resistance

The interest in estimating the ultimate side friction was aroused in 1960s when instrumented well-performed field tests showed the high ratio of rock socket resistance to total head load (Seol *et al.*, 2009; Ye *et al.*, 2013). Accurate assessment of ultimate status provides useful economical deign to achieve significant cost benefits. The peak unit side resistance can be estimated from a correlation method based on uniaxial compressive strength or a theoretical method from the Hoek-M failure mechanism.

The Hoek-Brown criterion (Hoek *et al.*, 2002) proposed to determine strengths of hard rock mass was applied to estimate the side friction of soft rock due to lack of suitable alternation. The modified Hoek-Brown criterion is showed as follows:

$$\frac{\sigma_1-\sigma_3}{\sigma_c}=(m\frac{\sigma_3}{\sigma_c}+s)^a \tag{5}$$

where σ_1 is the major principal stress at failure; σ_3 is the minor principal stress; σ_c is the uniaxial compressive strength of intact rock; and *m, s,* and *a* are the constants depending on the characteristics of the rock mass.

Based on the Geological Strength Index (GSI) rock mass classification and the Hoek-Brown criterion, Myung and Paik (2007) proposed a new criterion by assuming smooth pile/rock interface, uniform force transfer, well-constructed bored hole and rock mass failure. In addition, the horizontal stress is equal to the vertical stress as the arch effect is ignored for simplicity. The new criterion is showed as follows:

$$\tau_{\max}=q_s=\frac{1}{2}\sigma_c(m_b\frac{\sigma_v}{\sigma_c}+s)a>\frac{\sigma_c D}{4L} \tag{6}$$

$$\sigma_v=H_s\lambda_s+H_r\lambda_r \tag{7}$$

$$m_b=m_i\exp\frac{GSI-100}{28} \tag{8}$$

$$s=\exp\frac{GSI-100}{9},\ a=0.5;\ GSI>25 \tag{9}$$

$$s = 0,\ a = 0.65 - \frac{GSI}{200};\ GSI < 25 \tag{10}$$

where τ_{max} and q_s is the ultimate side friction; σ_v is the overburden stress; D is the diameter of the pile; and j and L is the length of the rock socket. H_r, H_s is the thickness of the rock layer and soil layer, respectively; λ_r, λ_s is the unite weight of rock and soil, respectively. GSI, m_i can be derived from the rock surface condition by lab tests or empirical value (Hoek *et al.*, 2002).

The difficulty of the new criterion was the definition of GSI and m_i owing to the high costs and complex experimental procedures to calculate them, which increases the uncertainty in estimating the side friction of drilled rock-socketed shaft and limit the application of this criterion.

The relatively easier correlation method based on UCS has been widely used since its emergence in 1970s owing to its easy operation and use of few indexes. The popular correlation is showed as follows:

$$q_s = \alpha \sigma_c^{\ n} \tag{11}$$

where σ_c is the unconfined compressive strength of intact rock (MPa); α is a reduction coefficient affected by mass rock quality, initial normal stress of concrete, diameter of shaft, pile-rock surface and uniaxial compressive strength; and n is an index ranging from 0.45 to 0.6 in general. With the technological and theoretical development, many scholars have improved the empirical correlation based on field and indoor tests and put forward more practical and accurate coefficients (Horvath and Kenney, 1979; Rowe and Armitage, 1987; Kulhway and Phoon, 1993; Ng *et al.,* 2001; Charif *et al.*, 2010).

From the table we could figure out the empirical correlations are based on different ultimate criteria at different sites. Hence, these models should be applied into Qingdao with more caution.

The database of 53 rock-socket piles from 7 field sites in Qingdao includes information of rock type, pile length, pile diameter, rock depth, rock compressive strength, side resistance, base resistance and construction method. The distributions of pile length, pile diameter, and rock compressive strength are presented in Tables 5 to 7, respectively. All the average UCS in this table is gained from the point loading test.

Table 5. Pile Length in Database

L/m	$0 < L \le 10$	$10 < L \le 20$	$20 < L \le 30$
Numbers	2	30	21
Percentage	4%	57%	39%

Table 6. Pile Diameter in Database

D/m	$0 < D \le 1$	$1 < D \le 2$	$2 < D \le 3$
Numbers	33	16	4
Percentage	62%	31%	7%

Table 7. Rock Unconfined Compressive Strength in Database

UCS/MPa	$0 < UCS \le 5$	$5 < UCS \le 10$	$10 < UCS \le 20$
Numbers	30	25	8
Percentage	56%	48%	14%

The performance of existing sample models was compared with the measured values from field tests in literatures. The plots of measured versus predicted side resistance along rock-socket shaft in Tables 5–7 are presented in Fig. 10. At each figure, the average and coefficient of variation of the ratio of predicted skin friction are presented to reflect model uncertainty related with each of empirical models.

Except the models proposed in 2010 and 2001, all other models tend to overestimate the side resistance slightly, with bias ranging from 1.62–1.98 (1979), 1.67–3.86 (1993) and 2.3–3.67 (1987). Such high deviations are expected since these models use different ultimate criterion at different sites. While the relatively new models (2010 and 2001) provide consistent measurements and predictions, with the average predicted to measured ratio of 1.62 and 1.64 respectively. This also indicates that test data from these models relatively come from similar sites and adopt the ultimate criterion based on head displacement. In addition, we could figure out these empirical models fit better when the side resistance is less than 1000 kPa, while the empirical correlation would underestimate the side resistance by more than 1000 kPa.

The correlation coefficients representing the correlation between prediction and measurement are relatively low and range from 0.2 to 0.34, which could be expected by the fewer samples, different construction methods and complex ground condition at

Table 4. Correlation between Side Friction of Drilled Shafts in Rock and Unconfined Compressive Strength

Year	Correlation	Rock	UCS/MPa	Date base	Ultimate status
1979	$q_{max} = 0.2 - 0.3(\sigma_c)^{0.5}$	Shale or mudstone		49 field tests	Local rock :6mm
1987	$q_{max} = 0.375 - 0.6(\sigma_c)^{0.5}$	-		-	-
1993	$q_{max} = 0.225 - 0.625(\sigma_c)^{0.55}$	limerock	1-20	-	Failure
2001	$q_{max} = 0.2(\sigma_c)^{0.5}$	granite	6-50	Hong kong	10-13.5(1%D)
2010	$q_{max} = 0.18(\sigma_c)^{0.5}$	weak carbonate	1-7	BUbai-UAE	FM?group AB?

Note: The ultimate status means the status when the side resistance of the test pile is adopted as the maximum side resistance in each correlation.

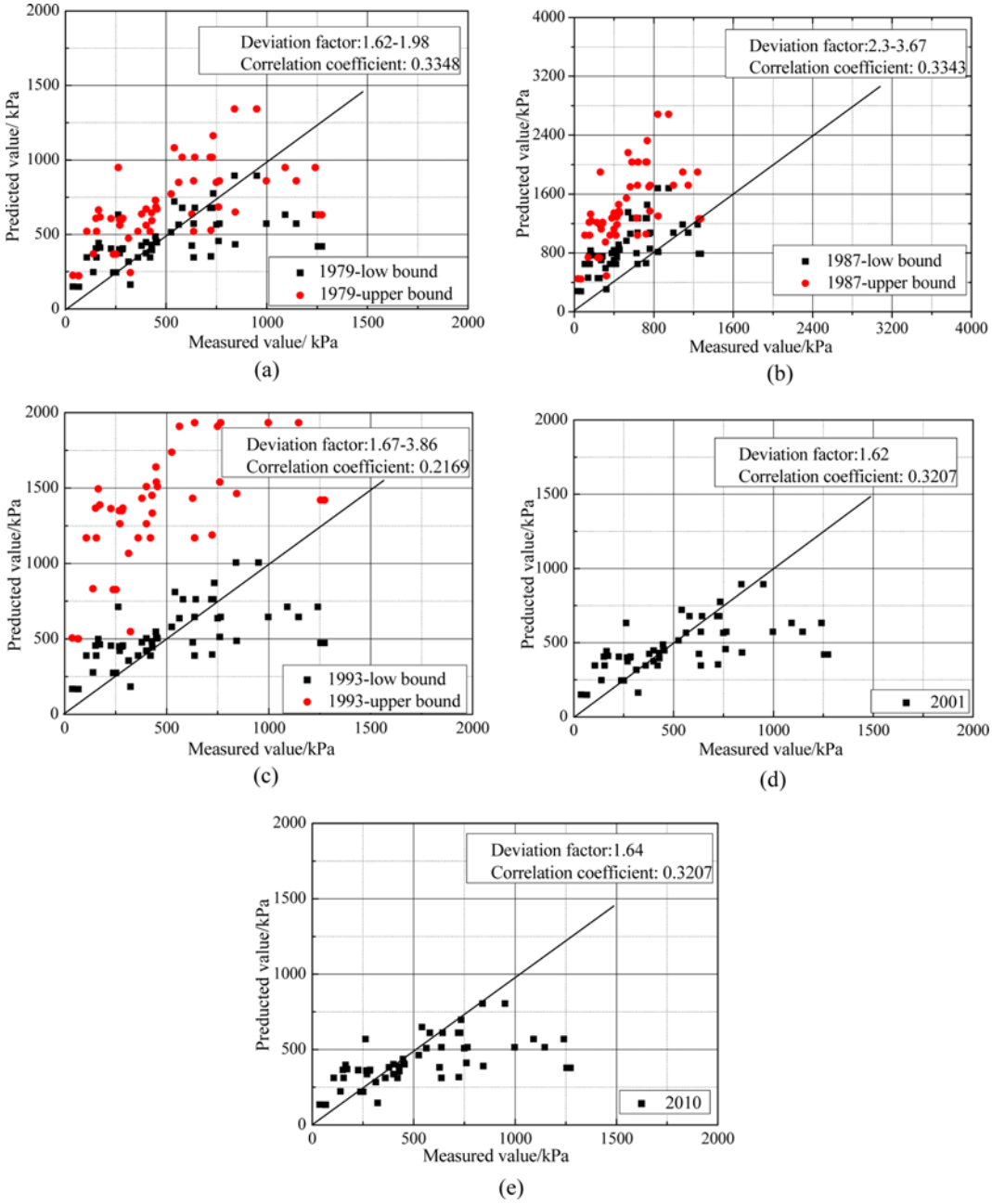

Where: deviation factor is the average ratio of max (prediction, measurement) to min (prediction, measurement)

Fig. 10. Performance of Existing Models for Predicting Side Resistance along Shaft into Rock

each site. The intact unconfined compressive strength is plotted against maximum measured side resistance in Fig. 11.

The new model (function y_1) is proposed by assuming the side resistance along shaft socket into rock only has relationship with rock layer and value of the side resistance and *UCS* collected in Qingdao is accurate and reliable. The parameter of α, n is determined when the deviation factor reaches minimum value. Hence, the new model could perform better at fitting side resistance along rocket part in Qingdao. Function y_2 and y_3 show the linear relationship between side resistance and unconfined compressive strength with $S/L > 0.6\%$ and $S/L < 0.6\%$, respectively. Because there are 1/2 testing piles (27 testing piles) having ratio of head sediment to pile length (S/L) up to 0.6%, we chose the 0.6% as the critical value.

As shown in Figs. 11 and 12, (1) a larger normalized displacement presents a relatively higher side friction under the same unconfined compressive strength, which can be explained by the fact that the fully-mobilized side resistance needs larger head displacement. (2) New models fitted data better at *UCS* < 4 MPa and > 10 MPa (deviation factor = 1.55), showed unsatisfactory fitting results at *UCS* of 4–10 (deviation factor = 1.73), which accords with other empirical correlation models.

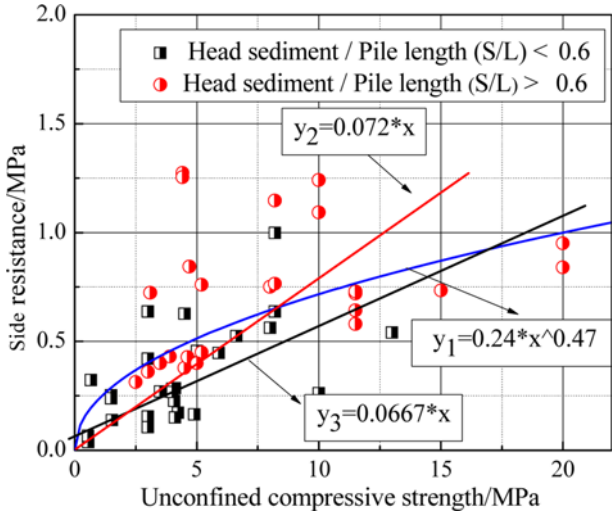

Fig. 11. Relationship between *UCS* and Peak Side Resistance

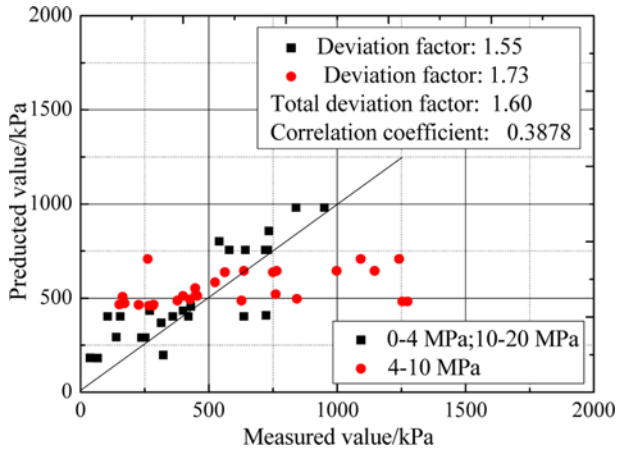

Fig. 12. Performance of Present Models for Predicting Side Resistance along Shaft into Rock

With the new correlation model, the average predicted side resistance of three piles with *UCS* of 3.5 and 11.5 MPa was 432 and 756 kN, respectively, and the measured value was 440 kN and 750 kN, respectively, which indicates the well estimation of the new correlation.

We could find that the new correlation is easy to operate and calculate. Besides, the new model has high applicability for Qingdao. However, there are only 53 piles being studied in the paper, adding the contingency of the research. It's also imprudent to ignore factors like *GSI*, the initial stress.

5. Conclusions

1. About 50% of head load is supported and transmitted by base resistance at the end of tests, which is relatively higher than previous studies. The obvious reduction of axial force at rock-socket part highlights the importance of accurately assessing side resistance along rock-socketed shaft.
2. Three test rock-socket piles tend to have a slow-type head displacement curve, with a high unload resilience more than 50%.
3. By comparing the predictions and measurements based on 53 test piles at Qingdao, we found the empirical correlation models proposed in 1987, 1993 and 1979 significantly overestimated the side resistance, with bias more than 3. The models proposed in 2001 and 2010 performed better except the underestimation of more than 1000 kPa.
4. The correlation between *UCS* and side resistance partly depends on the normalized displacement. Larger *S/L* indicating full mobilization shows a higher side resistance at the same condition. A new empirical method was put forward to fit the geological condition at Qingdao.

Acknowledgements

The funding support from National Natural Science Foundations of China (No.51078196 & No.41502304), Collaborative Innovation Center of Engineering Construction and Safety in Shandong Blue Economic Zone, China and Qingdao University of Technology, China are gratefully acknowledged.

References

Charif, K. H., Najjar, S. S., and Salah, S. (2010). "Side friction along drilled shafts in weak carbonate rocks." *Proc. Art of Foundation Engineering Practice*, pp. 190-205.

Dai, G. L., Bouncheloukh, A., and Gong, W. M. (2013). "Review of design methods of the ultimate side shear and base resistance for rock-socketed pile." *Applied Mechanics and Materials*, No. 353, pp. 60-67, DOI: 10.4028/www.scientific.net/AMM.353-356.60.

Fatahi, B., Basack, S., and Ryan, P. (2014). "Performance of laterally loaded piles considering soil and interface parameters." *Geomechanics and Engineering,* Vol. 7, No. 5, pp. 495-524, DOI: 10.12989/gae.2014.7.5.495.

Fellenius, B. H., Harris, D. E., and Aanderson, D. G. (2004). "Static loading test on a 45 m long pipe pile in Sandpoint Idaho." *Canadian Geotechnical Journal*, Vol. 41, No. 4, pp. 613-628, DOI: 10.1139/t04-012.

Gong, C. Z., Gong, W. M., and He, C. L. (2011). "Influence of hole side roughness on bearing characteristic of deep rock-socketed pile." *China Journal of Highway and Transport*, Vol. 24, No. 2, pp. 56-61.

Han, F., Prezzi, M., and Salgado, R. (2016). "Axial resistance of closed-ended steel-pipe piles driven in multilayered soil." *Journal of Geotechnical and Geoenvironmental Engineering,* pp. 102-106, DOI: 10.1061/(ASCE) GT.1943-5606.0001589.

Hoek, E., Carranzza-Torres, C., and Corkum, B. (2002). "Hoek-Brown failure criterion-2002 edition." *Proc. NARMS-Tac*., No. 1, pp. 267-273.

Horvath, R. G. and Kenney, T. C. (1979). "Shaft resistance of rock-socketed drilled piers." *Symposium on Deep Foundations*, pp. 182-214.

Kou, H. L., Guo, W., and Zhang, M. Y. (2016). "Axial resistance of long rock-socketed bored piles in stratified soils." *Ocean Engineering*, No. 114, pp. 58-65, DOI: 10.1016/ j. oceaneng. 2016.01013.

Kulhawy, F. H. and Phoon, K. K. (1993). "Drilled shaft side resistance in clay soil to rock." *Design and Performance of Deep Foundations,* No. 38 pp.172-183.

Kulkarni, R. U. and Dewaikar, D. M. (2016). "An empirical approach to assess socket friction and point resistance of axially loaded rock-socketed piles of Mumbai region." *International Journal of Geotechnical Engineering*, pp. 1-8, DOI: 10.1080 /19386362.2016.1237607.

Luo, Y., Li, C. F., and Xing, H. F. (2014). "Research on bearing behaviors of large-diameter rock-socketed piles through distributed optical fiber sensing technology." *Rock and Soil*, Vol. 35, No. 5, pp. 1406-1412.

Myung, S., Kyuho, P., and Deehyeon, K. (2007). "A new approach to estimate side resistance of rock-socketed drilled shafts." *Soils and Foundatio*n, Vol. 47, No. 2, pp. 415-421, DOI: 10.3208/sandf.47.415.

Ng, C. W. W., Yau, T. L. Y., and Li, J. H. M. (2001). "Side resistance of large diameter bored piles socketed into decomposed rock." *Journal of Geotechnical and Geoenvironmental Engineering*, Vol. 127, No. 8, pp. 642- 657, DOI: 10.1061/(ASCE)1090-0241(2001)127:8(642).

Nguyen, L., Fatahi, B., and Khabbaz, H. (2017). "Development of a constitutive model to predict the behavior of cement-treated clay during cementation degradation: C3 model." *International Journal of Geomechanics*, Vol. 17, No. 7, pp. 04017010-04017031.

The Professional Standard Compilation Group of People's Republic of China (2008). *JGJ94-2008 Technical code for building pile foundation*, S. Beijing: Architecture and Building Press.

The Professional Standards of People's Republic of China (2014). *JGJ106-2014 Technical code for testing of building foundation piles*, S. Beijing: China Architecture and Building Press.

Rowe, R. K. and Armitage, H. H. (1987). "Theoretical solutions for axial deformation of drilled shafts in rock." *Canadian Geotechnical Journal*, Vol. 24, No. 1, pp. 114-125, DOI: 10.1139/t87-010.

Seol, H., Jeong, S., and Cho, S. (2009). "Analytical method for load-transfer characteristics of rock-socketed drilled shafts." *Journal of Geotechnical and Geoenvironmental Engineering*, Vol. 135, No. 6, pp. 778-789, DOI: 10.1061/(ASCE) 1090-0241(2009)135:6(778).

Shi, P. D. and Lin, J. Y. (1994). "Vertical bearing capacity of rock-socketed piles." *Chinese Journal of geotechnical engineering,* pp .4.

Wang, W. D., Wu, J., and Nie, S. B. (2015). "Field loading tests on large-diameter rock-rocketed bored piles of Wuhan Greenland Center Tower." *Chinese Journal of Geotechnical Engineering*, Vol. 37, No.11, pp. 1945-1954.

Xing, H., Zhang, Z., and Meng, M. (2014). "Centrifuge tests of super large-diameter rock-socketed piles and their bearing characteristics." *Journal of Bridge Engineering*, Vol. 19, No. 6, pp. 10-14, DOI: 10.1061/ (ASCE) BE. 1943-5592.0000582.

Yan, N., Bai, X. Y., and Shui, W. H. (2015). "In-situ test study on vertical compressive bearing capacity characteristic of large diameter super-long impact-cone concrete pile." *Journal of Central South University (Science and Technology)*, Vol. 46, No. 7, pp. 2571-2580.

Ye, G. B., Meng, M. H., and Xing, H. F. (2013). "Side friction analysis of rock-socketed pile considering dilatancy of structural plane." *Chinese Journal of Rock Mechanics and Engineering*, Vol. 32, No. 5, pp. 909-916.

Zhang, L. (2010). "Prediction of end-bearing capacity of rock-socketed shafts considering Rock Quality Designation (RQD)." *Canadian Geotechnical Journal,* Vol. 47, No. 10, pp. 1071-1084, DOI: 10.1139/T10-016.

Zhao, M. H., Lei, Y., and Liu, X. M. (2009). "Analysis of load transfer of rock-socketed piles based on characteristics of pile-rock structural plane." *Chinese Journal of Rock Mechanics and Engineering*, Vol. 28, No. 1, pp. 103-110.